Surface Charge Deposition by Moving Drops Reduces Contact Angles

Xiaomei Li,[1,*] Aaron D. Ratschow,[2,*] Steffen Hardt,[2,†] and Hans-Jürgen Butt[1,‡]
[1]Max Planck Institute for Polymer Research, Ackermannweg 10, 55128 Mainz, Germany
[2]Institute for Nano- and Microfluidics, TU Darmstadt, Peter-Grünberg-Str. 10, D-64289 Darmstadt, Germany

(Received 6 April 2023; accepted 19 October 2023; published 28 November 2023)

Slide electrification—the spontaneous charge separation by sliding aqueous drops—can lead to an electrostatic potential in the order of 1 kV and change drop motion substantially. To find out how slide electrification influences the contact angles of moving drops, we analyzed the dynamic contact angles of aqueous drops sliding down tilted plates with insulated surfaces, grounded surfaces, and while grounding the drop. The observed decrease in dynamic contact angles at different salt concentrations is attributed to two effects: An electrocapillary reduction of contact angles caused by drop charging and a change in the free surface energy of the solid due to surface charging.

DOI: 10.1103/PhysRevLett.131.228201

Drops moving on solid surfaces play a fundamental role in many natural and technological processes from raindrops spreading on plant leaves or glass to processes like inkjet printing or coating [1–3]. Wetting phenomena are characterized by contact angles. Young's equation relates the contact angle (θ) to the interfacial energies of the liquid surface (L), solid surface (S), and the solid-liquid interface (SL) with [4],

$$\gamma_{\mathrm{L}} \cos\theta = \gamma_{\mathrm{S}} - \gamma_{\mathrm{SL}}. \tag{1}$$

Because higher solid surface energies cause lower contact angles, wettability can be controlled by choosing high or low surface energy materials.

To control and switch contact angles, electrowetting is a versatile tool, used in various microfluidic applications [5]. In electrowetting, a drop is placed on a thin dielectric layer on a flat electrode. The contact angle decreases when a voltage (ΔV) is applied between the drop and the electrode. Microscopically, this effect is caused by the Maxwell stress acting on the liquid surface near the contact line. Macroscopically, it can be attributed to a change in solid-liquid interfacial energy [6,7]. It is energetically favorable for countercharges to accumulate at the solid-liquid interface under an applied potential, and thus its surface energy is reduced by

$$\Delta\gamma_{\mathrm{SL}} = \gamma_{\mathrm{SL}}^{\mathrm{eff}} - \gamma_{\mathrm{SL}} = -\frac{\varepsilon_0 \varepsilon_r}{2d} \Delta V^2. \tag{2}$$

This decrease depends on the permittivity (ε_0 = vacuum permittivity, ε_r = relative permittivity) and the thickness of the dielectric layer d separating the liquid from the flat electrode [5]. The change in contact angle is given by the Young-Lippmann equation [6],

$$\cos\theta - \cos\theta' = \frac{\Delta\gamma_{\mathrm{SL}}}{\gamma_{\mathrm{L}}}. \tag{3}$$

Here, θ and θ' are the contact angles without and with an applied voltage.

For drop motion, however, the advancing (θ_a) and receding contact angles (θ_r) are relevant. In contrast to the equilibrium contact angle, they are measurable. Advancing contact angles are measured at the front, receding contact angles at the backside of a drop. The friction force, which resists sliding, can be described by [8,9]

$$F = w\gamma_L k(\cos\theta_r - \cos\theta_a), \tag{4}$$

with drop width w and a geometrical factor $k \approx 1$ [10,11]. Since friction increases with velocity, it is commonly accepted that θ_a increases and θ_r decreases with velocity. Thus, the difference between the two, the contact angle hysteresis $\theta_a - \theta_r$, increases. By assuming a local equilibrium we apply Eqs. (1)–(3) to θ_a and θ_r separately.

In slide electrification, a sliding aqueous drop on a hydrophobic surface usually charges positively while leaving behind an opposite charge on the dewetted surface [12–19]. Spontaneous charging of moving drops influences their motion substantially by electrostatic forces [14]. However, it is still unclear if spontaneous charging also changes the contact angle. If so, this would fundamentally affect contact angle hysteresis [20]. Previous experiments [14] were carried out with distilled water. Here, we added salt. In addition, we carried out experiments in which

the drop was grounded while sliding. We address the questions: Do charges in the drop and/or surface charges generated by slide electrification change the advancing and receding contact angles? If yes, how does this effect depend on the salt concentration?

To answer these questions, we imaged sliding aqueous drops (Supplemental Material, S1 [21]) in a custom-made tilted plate setup [Fig. 1(a)] [14]. 30 μL drops were placed onto a tilted surface by a peristaltic pump with a grounded syringe needle at fixed intervals of 1.5 s. The sliding time of each drop was around 0.15 s, short enough to ignore the influence of surface discharging [13] and evaporation [22]. The surfaces were flat and hydrophobic, with an average roughness < 1 nm within an area of 0.5×0.5 μm^2 (Supplemental Material, S2 and S3 [21]). Every drop moving down the surface first contacted a grounded electrode. We imaged the sliding drops from the side with a high-speed camera. We set the slide length and time to zero when drops detached from the grounded electrode and enter the recording window. At this point, they already had an initial velocity. An adapted image analysis MATLAB code [23] extracted the positions, velocities, and advancing and receding contact angles from the side-view images. The drop velocity for every position was defined as the mean of the advancing and receding contact line velocities. Charge measurements were conducted with a current amplifier connected to a wire electrode after sliding for 4 cm (Supplemental Material, S4 [21]). As surfaces, we prepared 60 nm thick Teflon films on quartz plates (Teflon-quartz) by dip coating (1 cm/ min) from a solution of 1 wt% Teflon AF 1600 and annealing at 160 °C under vacuum for 24 h. The quartz plates were 1 mm thick and placed on a grounded metal plate.

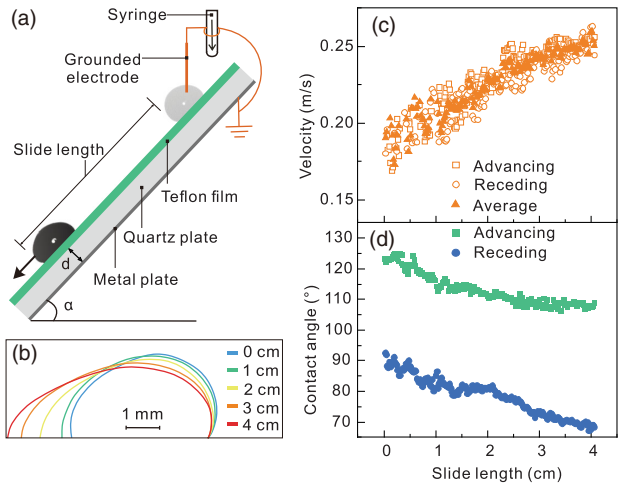

FIG. 1. Experiments for a 30 μL aqueous drop with 1 mM NaCl on initially uncharged Teflon quartz without grounding while sliding. (a) Schematic of the experimental setup. (b) Drop profiles for different values of the slide length, (c) drop velocity, (d) dynamic advancing, and receding contact angle.

When placing an aqueous drop containing 1 mM NaCl on a pristine, uncharged Teflon-quartz surface [Fig. 1(a)], the drop accelerates. Its shape elongates [Fig. 1(b)] while the velocity increases [Fig. 1(c)]. Additionally, the dynamic advancing and receding contact angles decrease with increasing velocity [Fig. 1(d)]. Established theories, like the Cox-Voinov hydrodynamic model [24,25], the molecular kinetic model [26], combinations of both [27,28], and the adaptation model [29] predict a decrease in receding, but an increase in advancing contact angle with increasing velocity. This does not agree with our measurements. We conclude that there are additional effects influencing the contact angles and propose that the change in contact angle is due to drop charging.

To verify drop charging causes this change in contact angles, we sputter-coated the quartz plates with 5 nm chromium and 35 nm gold before coating Teflon films on top (Teflon-gold). In earlier experiments we had shown that contrary to Teflon-quartz [Fig. 2(a)], charging is negligible for 50 nm polymer films on grounded gold [Fig. 2(b)] [14]. For Teflon-gold, the advancing contact angle indeed increases with velocity [Fig. 2(e), orange symbols] and the decrease of the receding contact angle is weaker [Fig. 2(f), orange symbols].

We propose that electrowetting reduces the contact angles of charged drops. The sliding drop on Teflon-quartz acquires positive charges, leaving negative surface charges behind. The related electrostatic potential leads to an electrowetting effect. To support this hypothesis, we calculate $\Delta\gamma_{SL}$. First, we convert drop charges Q

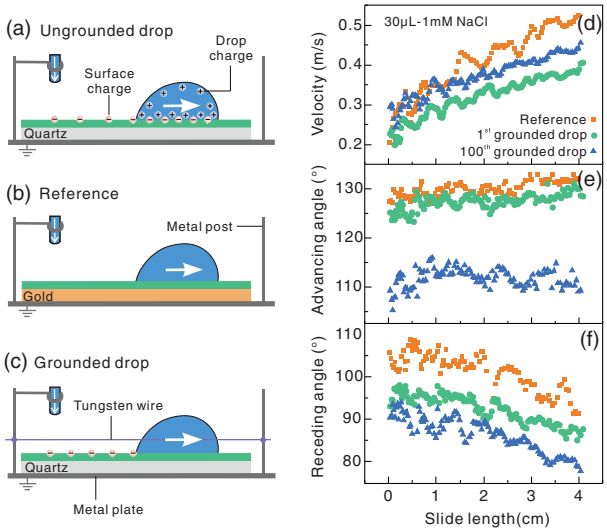

FIG. 2. Dynamic contact angles reduced by slide electrification. Schematics of a drop sliding down the 40° tilted (a) Teflon-quartz surface and (b) Teflon-gold surface without drop grounding, and (c) Teflon-quartz surface with drop grounding during sliding. The corresponding drop velocity (d), dynamic advancing contact angle (e), and dynamic receding contact angle (f) over slide length for the 1st and 100th consecutive drop.

to a potential $\Delta V = Q/C$ with the drop capacitance $C = A\varepsilon_0\varepsilon_r/d$ (Supplemental Material, S5 [21]). Here, A is the contact area of the drop. The dielectric capacitance dominates the capacitance [5]. In previous measurements [14], after 4 cm sliding on Teflon-quartz the charge of the 1st drop was $Q \approx 0.7$ nC, $A \approx 17$ mm^2 and $\varepsilon_r = 4.5$. We estimate $\Delta V \approx 1$ kV, comparable to potentials reported by [30]. Based on Eq. (2), the change in solid-liquid interfacial tension is roughly 20 mN/m, leading to a contact angle decrease of ≈18°. Since the drop continuously deposits charges while sliding [13], its potential increases with slide length. Electrowetting can thus explain the decrease in advancing contact angle.

Are there other electrostatic effects influencing the contact angles? To isolate such effects, we used the same Teflon-quartz surfaces but grounded the sliding drop with a tungsten wire to prevent drop charging and electrowetting effects [Fig. 2(c)]. The grounded tungsten wire (25 μm diameter), spanned at ≈1 mm height above the surface, had negligible influence on the drop motion (Supplemental Material, S6 [21]). The grounded drop could still deposit negative surface charge at its rear, but itself remained uncharged.

Figures 2(d)–2(f) show the velocity, and the dynamic advancing and receding contact angles versus slide length for the 1st and 100th consecutive grounded drop on Teflon-quartz. We observe a distinct difference between the 1st (green circles) and 100th (blue triangles) drop. This indicates that the surface charge on the solid-air interface influences the contact angles and drop motion, even if the drop is uncharged. The results on Teflon-gold (orange circles) are plotted for reference. There is no significant difference between the 1st and 100th drop on Teflon-gold (Supplemental Material, S7 [21]).

Compared with the Teflon-gold reference [Figs. 2(e)–2(f), orange], the dynamic advancing contact angle of the 1st grounded drop on Teflon-quartz was not significantly affected by electrostatic effects. Only the dynamic receding contact angle was reduced by 10°. In comparison, the dynamic advancing contact angle of the ungrounded drop [Fig. 1(d)] decreased for slide lengths > 0 as the drop charged and electrowetting commenced. For the 100th grounded drop on Teflon-quartz [Figs. 2(e)–2(f), blue], both the dynamic advancing and receding contact angles deviated from the Teflon-gold reference. The main difference was that the grounded drop continuously deposited charges at its receding contact line [Figs. 2(b)–2(c)] while no charging occurred on Teflon-gold. Thus, in addition to electrowetting, surface charges cause a fundamentally new electrostatic effect that decreases contact angles.

We propose that charges on the solid-gas interface increase the surface energy and according to Young's equation reduce the contact angles. The surface energy increases by two effects. First, the self-energy of the charges on the surface. The corresponding change in the surface energy is, however, only of the order of 10 μN/m (Supplemental Material, S8 [21]) and is thus negligible. Second, surface charges electrostatically repel each other. Thus, forming a layer of charges requires electrostatic work. We derived a theoretical scaling for this effect based on the work required to deposit an additional elementary charge on a charged surface. This energy depends on the size of the charged patch. Exemplarily, we consider a circular patch with radius R and a charge density σ. After area averaging this energy, the change in free surface energy of the solid due to the presence of a charge density is (Supplemental Material, S8 [21]):

$$\Delta\gamma_S = \gamma_S^{\text{eff}} - \gamma_S = \frac{\sigma^2 R}{\varepsilon_0(1+\varepsilon_r)}. \tag{5}$$

The corresponding contact angle change is

$$\cos\theta - \cos\theta' = -\frac{\Delta\gamma_S}{\gamma_L}. \tag{6}$$

The surface energy increases quadratically with the charge and linearly with the size of the charged area R. For an estimate, we set R equal to the drop radius. With $R = 2$ mm and a charge density of $\sigma = 10$ μC/m^2 [14], $\Delta\gamma_S$ is of the order of 10 mN/m, which would substantially change contact angles. Equations (5) and (6) apply to both advancing and receding contact angles by inserting the surface charge density before and behind the drop, respectively.

Analogous to the electromechanical interpretation of electrowetting, a meaningful apparent contact angle can only be defined above the length scale of the electrostatic interaction. Above the length scale of surface forces (≈10 nm), electrostatic forces, expressed by the Maxwell stress, and capillary forces balance at the liquid-air interface. In electrowetting on dielectric, the Maxwell stress is typically localized to a few μm near the contact line due to the thickness of the dielectric film [5]. Here, with the grounded flat electrode being millimeters away, the electrostatic problem of an isopotential wedge, representing the liquid, next to a charged surface (Fig. 3) does not have an inherent length scale. Thus, there is no apparent length scale over which the Maxwell stress is localized. It even becomes singular at the contact line [14,31] for the model problem of an isopotential wedge.

Since singularities do not occur in nature, the question arises about a microscopic length scale that cuts off the singularity. Different mechanisms could introduce a microscopic length scale close to the contact line. First, treating the liquid surface as isopotential only applies on length scales above the Debye length, $\lambda \approx 1$–1000 nm in aqueous solutions. Second, singularities of the electric field at the contact line would lead to electrostatic discharge [32,33] above the limiting field strength of humid air, ≈2 MV/m [34]. Any singularity would be eliminated

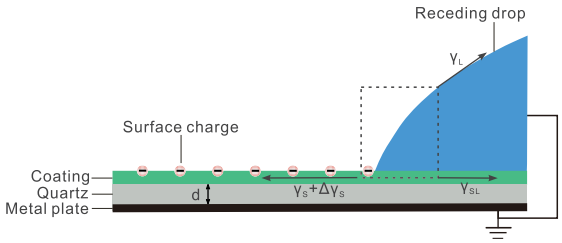

FIG. 3. Schematic representation of contact-angle modification via electrostatic interaction with surface charges. Deposited charges deform the liquid surface via electrostatic interaction. Above a characteristic length scale ("control" volume indicated by a dashed rectangle), the effect can be subsumed as a change in solid surface energy.

on a length scale where electrostatic discharge occurs. With numerical simulations, we show that such a microscopic length scale strongly localizes the Maxwell stress to a limiting length scale of the order of 1 μm (Supplemental Material, S9 [21]). Above 1 μm, the apparent contact angle should be well defined by a change in the effective solid surface energy (Fig. 3).

To explain the change of dynamic contact angles, we consider three effects: (i) Nonelectrostatic contributions [24–29], (ii) surface charge-induced changes of the solid surface [Eq. (5)], and (iii) electrowetting due to drop charging [Eq. (2)]. Our experiments are designed such that the reference measurement on Teflon-gold is only influenced by (i). On Teflon-quartz, the grounded drop is influenced by (i) and (ii), and the ungrounded drop is influenced by (i)–(iii). The initial decrease in receding contact angle between the reference and the grounded drop for the 1st drop was around 10° [Fig. 2(f)]. To fully explain this with Eq. (5), the drop with a radius of 2 mm on quartz ($\varepsilon_r = 4.5$) would have to deposit a surface charge of $\sigma = 16\ \mu\mathrm{C/m^2}$. This value agrees magnitudewise with our previously published measurement of $10.3\ \mu\mathrm{C/m^2}$ on the same substrate [14].

For the 100th drop (blue) shown in Figs. 2(e)–2(f), also the advancing contact angle decreased. We attribute this to surface charges deposited by previous drops.

Because of hydrodynamics, contact-line friction, and adaptation (effect i), receding contact angles are lower than advancing contact angles. Dynamic receding contact angles are more affected by surface charge than advancing ones. In line with this observation, Eqs. (5) and (6) predict that lower contact angles are affected more [Fig. 4(a)]. Note that the applicability of such models becomes questionable for contact angles of 20°–30° due to electrostatic discharge [32].

The theory predicts a scaling of the effect with the size of the charged area, that for the first drop corresponds to the drop radius R. To confirm this, we plotted $\cos(\theta') - \cos(\theta)$ measured with grounded drops of different volumes V. As predicted by Eqs. (5) and (6), an increase with $R \propto V^{1/3}$ was observed. For volumes > 30 μL, the simple scaling breaks down as the Bond number $\mathrm{Bo} = \rho g H^2/\gamma_L$ (ρ: liquid density, g: gravitational acceleration, H: characteristic drop radius) approaches unity [Fig. 4(b), Supplemental Material, S11 [21]]. Gravity becomes dominant, reflected in higher experimental values.

The reduction of dynamic contact angles increases with increasing salt concentration up to ≈1 mM followed by a decrease [Figs. 4(c) and S11b in [21]]. This trend is consistent with reported drop or surface charges [35–37]. The initial increase with salt concentration can be explained by the Péclet number dependency of charge separation. In the drop, there is a flow component directed upward at the receding contact line. It drives counterions away from the surface and extends the effective screening length. Assuming charge regulation at the solid-liquid interface, an extended screening length reduces the surface charge at the receding contact line and thus the deposited surface charge. This mechanism is only effective when convective transport is stronger than ion diffusion. The Péclet number $\mathrm{Pe} = U\lambda/D$ (U = drop velocity, D = salt diffusivity [38]) measures convective transport, which is of minor importance up to $\mathrm{Pe} = 1$ and decreases charge separation for $\mathrm{Pe} > 1$ [39]. For typical values $U = 0.3$ m/s and $D = 1.6 \times 10^{-9}\ \mathrm{m^2/s}$, a transition between the two regimes occurs at a salt concentration of 3 mM (2–4 mM,

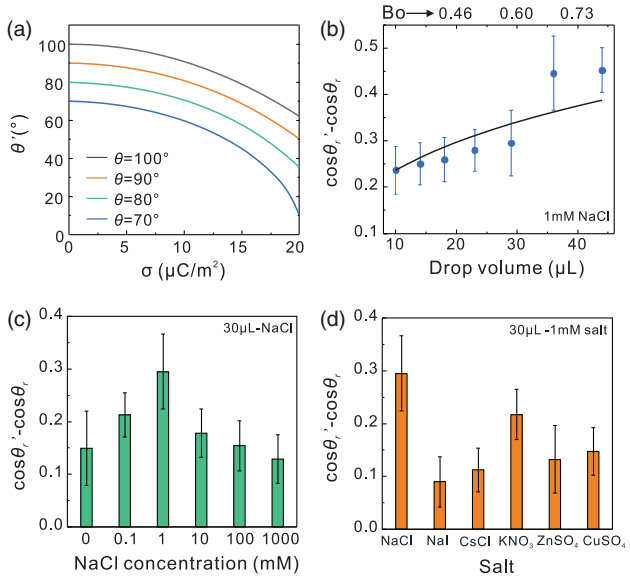

FIG. 4. Universality of the effect. (a) Theoretically expected contact angle as a function of surface charge density for different initial contact angles and a drop radius of 2 mm, calculated with Eqs. (5) and (6). Experimentally determined $\cos(\theta_r') - \cos(\theta_r)$ for the first grounded drops with (b) different drop volumes, (c) salt concentrations, and (d) salt types on pristine Teflon-quartz surfaces in the velocity range 0.3–0.4 m/s. θ_r and θ_r' are the dynamic receding contact angles without and with slide electrification. Error bars represent the Gaussian error propagation of the standard deviation between three measurements.

Supplemental Material, S11, Table S1 [21,40]), which explains the reduced contact angle changes at ≤ 1 mM. The experimental trends are in accordance with the theoretical scaling.

We demonstrate the universality of the effect by measuring surfaces with different coatings, including 35 nm thick polystyrene (PS) films quartz plates coated with, molecular layers of perfluoroctyltriethoxysilane (PFOTS), and polydimethylsiloxane (PDMS) grafted to quartz plates (Supplemental Material, S10 [21]) and drops with different salts (Figs. 4 and S11a in [21]). While the exact nature and even sign of surface charge could change due to specific adsorption of ions, different reactive surface groups, or different points of zero charge, the contact angle decrease described here only hinges on the surface charge magnitude.

In addition to our own measurements, our theory helps to explain observations from the literature. Mugele *et al.* [41] reported that the contact angle of an aqueous solution on Teflon permanently decreased by 5°–10° after the first wetting-dewetting cycle. This was likely caused by charges deposited onto the surface during the initial dewetting. Sun *et al.* [42] experimentally demonstrated that drops move along surface charge gradients towards higher charged regions, even against gravity. This is easily conceivable with Eq. (5), as the higher charged regions have an increased free surface energy. The universality of slide electrification and subsequent contact angle changes sheds new light on many works dealing with contact angle hysteresis on dielectrics substrates, where these effects likely played a role [43–46].

To conclude, we identified two mechanisms explaining how slide electrification can lead to a reduction in dynamic contact angles. First, charges in the drop induce an electric field between the drop and the subsurface electrode, which via electrowetting causes a reduction of contact angles. Second, charges on the solid surface effectively increase the surface energy and thus reduce the contact angle according to Young's equation. This can substantially reduce the dynamic and static contact angles, even when the drop is grounded. The discovered effect could help to explain contact angle hysteresis in many practical cases and facilitate the design of functional surfaces by focusing on the prevention of charge separation.

We wish to thank Rüdiger Berger, Diego Diaz, and Lisa S. Bauer for their valuable suggestions regarding the experiments and Tobias Baier for helpful discussions on the theory. H.-J. B. proposed and supervised the work, X. L. designed, conducted, evaluated, and interpreted the experiments, A. D. R. developed the theoretical framework with input from H.-J. B. and S. H. and derived the analytical model, A. D. R. and S. H. worked out the simulation model and conducted the simulations, X. L. and A. D. R. prepared the manuscript. This work was supported by the European Research Council (ERC) under the European Union's Horizon 2020 research and innovation program (Grant agreement No. 883631) (H.-J. B.), the Priority Programme 2171 "Dynamic wetting of flexible, adaptive and switchable surfaces" (Grant No. BU 1556/36: X. L., H.-J. B.), the Department for Process and Plant Safety of Bayer AG, Leverkusen, Germany (A. D. R.), and the German Research Foundation (DFG) within the Collaborative Research Centre 1194 "Interaction of Transport and Wetting Processes," Project- ID 265191195, subprojects A02b (S. H., A. D. R.) and C07 (H.-J. B.).

*These authors contributed equally to this work.
†hardt@nmf.tu-darmstadt.de
‡butt@mpip-mainz.mpg.de

[1] P.-G. Gennes, F. Brochard-Wyart, and D. Quéré, *Capillarity and Wetting Phenomena: Drops, Bubbles, Pearls, Waves* (Springer, New York, 2004).
[2] D. Bonn, J. Eggers, J. Indekeu, J. Meunier, and E. Rolley, Rev. Mod. Phys. **81**, 739 (2009).
[3] D. Lohse, Annu. Rev. Fluid Mech. **54**, 349 (2022).
[4] T. Young, Phil. Trans. R. Soc. London **95**, 65 (1805).
[5] F. Mugele and J. Heikenfeld, *Electrowetting: Fundamental Principles and Practical Applications* (John Wiley & Sons, New York, 2018).
[6] J. Buehrle, S. Herminghaus, and F. Mugele, Phys. Rev. Lett. **91**, 086101 (2003).
[7] F. Mugele and J. Buehrle, J. Phys. Condens. Matter **19**, 375112 (2007).
[8] A. Buzagh and E. Wolfram, Kolloid Z. **157**, 50 (1958).
[9] K. Kawasaki, J. Colloid Sci. **15**, 402 (1960).
[10] C. Antonini, F. J. Carmona, E. Pierce, M. Marengo, and A. Amirfazli, Langmuir **25**, 6143 (2009).
[11] S. Humayun, R. D. Maynes, J. Crockett, and B. D. Iverson, Langmuir **38**, 15960 (2022).
[12] K. Yatsuzuka, Y. Mizuno, and K. Asano, J. Electrost. **32**, 157 (1994).
[13] A. Z. Stetten, D. S. Golovko, S. A. Weber, and H.-J. Butt, Soft Matter **15**, 8667 (2019).
[14] X. Li, P. Bista, A. Z. Stetten, H. Bonart, M. T. Schür, S. Hardt, F. Bodziony, H. Marschall, A. Saal, X. Deng, R. Berger, S. A. L. Weber, and H.-J. Butt, Nat. Phys. **18**, 713 (2022).
[15] Y. Jin, C. Wu, P. Sun, M. Wang, M. Cui, C. Zhang, and Z. Wang, Droplet **1**, 92 (2022).
[16] J. K. Beattie, Lab Chip **6**, 1409 (2006).
[17] K. N. Kudin and R. Car, J. Am. Chem. Soc. **130**, 3915 (2008).
[18] C. Tian and Y. Shen, Proc. Natl. Acad. Sci. U.S.A. **106**, 15148 (2009).
[19] T. Preočanin, A. Selmani, P. Lindqvist-Reis, F. Heberling, N. Kallay, and J. Lützenkirchen, Colloids Surf. A **412**, 120 (2012).
[20] H. B. Eral, D. J. C. M. 't Mannetje, and J. M. Oh, Colloid Polym. Sci. **291**, 247 (2013).
[21] See Supplemental Material at http://link.aps.org/supplemental/10.1103/PhysRevLett.131.228201 for details in liquid and surface perforation; SFM and charge

measurement; calculation of the change in interfacial energies; influence of tungsten wire, polymer coating, salt type, salt concentration, and drop volume.
[22] V. Charitatos, T. Pham, and S. Kumar, Phys. Rev. Fluids **6**, 084001 (2021).
[23] N. K. Andersen and R. Taboryski, Meas. Sci. Technol. **28**, 047003 (2017).
[24] O. Voinov, Fluid Dyn. **11**, 714 (1976).
[25] R. Cox, J. Fluid Mech. **168**, 169 (1986).
[26] T. Blake and J. Haynes, J. Colloid Interface Sci. **30**, 421 (1969).
[27] F. Brochard-Wyart and P. De Gennes, Adv. Colloid Interface Sci. **39**, 1 (1992).
[28] P. Petrov and I. Petrov, Langmuir **8**, 1762 (1992).
[29] H.-J. Butt, R. Berger, W. Steffen, D. Vollmer, and S. A. L. Weber, Langmuir **34**, 11292 (2018).
[30] W. Xu, Y. Jin, W. Li, Y. Song, S. Gao, B. Zhang, L. Wang, M. Cui, X. Yan, and Z. Wang, Sci. Adv. **8**, eade2085 (2022).
[31] L. Y. Yeo and H.-C. Chang, Mod. Phys. Lett. B **19**, 549 (2005).
[32] M. Vallet, M. Vallade, and B. Berge, Eur. Phys. J. B **11**, 583 (1999).
[33] J.-M. Löwe, V. Hinrichsen, I. V. Roisman, and C. Tropea, Phys. Rev. E **102**, 063101 (2020).
[34] B. Li, X. Li, M. Fu, R. Zhuo, and D. Wang, J. Phys. D **51**, 375201 (2018).
[35] L. E. Helseth, Langmuir **36**, 8002 (2020).
[36] M. D. Sosa, M. L. M. Ricci, L. L. Missoni, D. H. Murgida, A. Cánneva, N. B. D'Accorso, and R. M. Negri, Soft Matter **16**, 7040 (2020).
[37] L. E. Helseth, Langmuir **39**, 1826 (2023).
[38] M. D. Morris and J. J. Lingane, J. Electroanal. Chem. (1959) **6**, 300 (1963).
[39] A. D. Ratschow, L. S. Bauer, P. Bista, S. A. L. Weber, H.-J. Butt, and S. Hardt, arXiv:2305.02172.
[40] C.-C. Chang, R.-J. Yang, M. Wang, J.-J. Miau, and V. Lebiga, Phys. Fluids **24**, 072001 (2012).
[41] F. Mugele, A. Klingner, J. Buehrle, D. Steinhauser, and S. Herminghaus, J. Phys. Condens. Matter **17**, S559 (2005).
[42] Q. Sun, D. Wang, Y. Li, J. Zhang, S. Ye, J. Cui, L. Chen, Z. Wang, H.-J. Butt, D. Vollmer, and X. Deng, Nat. Mater. **18**, 936 (2019).
[43] E. Schäffer and P. Z. Wong, Phys. Rev. Lett. **80**, 3069 (1998).
[44] A. Giacomello, L. Schimmele, and S. Dietrich, Proc. Natl. Acad. Sci. U.S.A. **113**, E262 (2016).
[45] H. Perrin, R. Lhermerout, K. Davitt, E. Rolley, and B. Andreotti, Phys. Rev. Lett. **116**, 184502 (2016).
[46] B. Dollet, É. Lorenceau, and F. Gallaire, Phys. Rev. Lett. **124**, 104502 (2020).